Volume 1 | Number 1 | Jan 2013 | Pages 1–100

PCCP

Physical Chemistry Chemical Physics
www.rsc.org/pccp

ROYAL SOCIETY OF CHEMISTRY

ROYAL SOCIETY OF CHEMISTRY

www.rsc.org/pccp

Journal Name

ARTICLE

A modelling approach for MOF-encapsulated metal catalysts and application to n-butane oxidation†

Diego A. Gomez-Gualdron,[a] Sean T. Dix,[b] Rachel B. Getman,[b*] and Randall Q. Snurr[a*]

Metal nanoparticles (NP) encapsulated by metal-organic frameworks (MOFs) are novel composite materials that have shown promise as regioselective catalysts. The regioselectivity in these materials arises from steric constraints imposed by the porous MOF structure, which limit the way molecules approach and interact with the metal surface. Here we introduce a conceptually simple DFT approach to model reactions under such steric constraints. This approach is computationally efficient and accounts for the steric constraints imposed by a MOF pore in a general way. The adsorption of reactants, intermediates, and products associated with oxidation of n-butane to 1-butanol (and 2-butanol) on clean and oxygen-covered palladium surfaces is investigated with (and without) the constraints of a pore. Reaction energies are calculated, and we find that the thermodynamic favorability of the intermediate reactions is affected by the presence of steric constraints, oxygen coverage, and the exposed crystal surface of the metal. Based on these results, the Pd(111) surface with 0.25 ML oxygen coverage and steric constraints (which could be provided by a suitable MOF) seems promising to favor the desired sequence of reactions that would lead to the conversion of n-butane to 1-butanol.

Introduction

Designing catalysts that are highly selective is one of the grand challenges in catalysis, and it is becoming increasingly important in the chemical industry, playing a key role in the development of "green" and economic processes for the production of commodity chemicals.[1-3] Highly selective processes reduce chemical waste and costly, energy-intensive separation processes associated with the formation of undesired products. A common strategy to improve the selectivity of heterogeneous catalysts has been to use strategically alloyed or doped versions of parent catalysts,[4-9] and theoretical methods such as density functional theory (DFT) have helped to identify promising compositions for reactions of interest.[4,10,11] However, alloying or doping by itself is often not sufficient to achieve the required selectivity.

Nature, in the form of enzymes, presents another working principle for highly selective reactions by controlling the orientation of reactants as they reach the (catalyst) active sites thus allowing only specific reactant regions to undergo catalytic conversion.[12] Although applying this principle in designing new heterogeneous catalysts remains a challenge, an interesting proposition is to surround catalyst particles with a porous shell[13-16] that could impart the desired orientation control. Metal-organic frameworks (MOFs) are attractive candidates for the porous shell material,

because they have uniform, highly tunable pore structures. MOF tunability originates from their modular structure, where different combinations of organic and inorganic "building units" can be assembled into different MOFs.[17-20] Indeed, the combinatorial possibilities are virtually unlimited, motivating the study of MOFs for applications such as gas storage,[21,22] separations,[23] and catalysis.[24]

In recent promising work, Lu et al.[16] developed a strategy for surrounding nanoparticles (NP) with a MOF to create so-called NP@MOF systems. Lu et al.[16] showed that a Pt@**ZIF-8** system could hydrogenate n-hexene, but not the bulkier cyclooctene, due to the size-selective nature of the surrounding MOF. More recently, Stephenson et al.[25] demonstrated that a Pt@**ZIF-8** system could regioselectively hydrogenate *trans*-1,3-hexadiene to 3-hexene. Here the terminal double bond was hydrogenated while the internal double bond was not, presumably because it could not access the metal catalyst surface due to steric constraints. Other recent examples of catalysis with NP@MOFs have been reported elsewhere.[26-35]

In light of these findings, an intriguing question is whether these NP@MOF systems can carry out more complex reactions. We are interested in designing a NP@MOF system to carry out the partial oxidation of a long alkane to its corresponding primary alcohol. This would allow, for instance, the production of 1-butanol—which is a widely used solvent and feedstock—through the partial oxidation of n-butane rather than through the hydroformylation of propylene[36] (a more expensive and scarce feedstock). The primary challenge is preventing the oxidation of the secondary carbon, whose C-H bonds are less stable than those of the primary carbon,[37] and the eventual formation of 2-butanol, which is

---

[a.] *Department of Chemical and Biological Engineering, Northwestern University. 2145 Sheridan Road, Evanston, IL 60208, USA. Email: Snurr@northwestern.edu*

[b.] *Department of Chemical and Biomolecular Engineering, Clemson University, 127 Earle Hall, Clemson, SC 29634, USA. Email: rgetman@clemson.edu*

† Electronic Supplementary Information (ESI) available: All optimized geometries, and more detailed information on adsorption and reaction energies. See DOI: 10.1039/x0xx00000

calculated to be 16 kJ/mol more stable than 1-butanol.[38] Additionally, overoxidation to CO_2 needs to be avoided.[39]

To address the above challenges, the structure of the surrounding MOF should be tuned so that only the terminal carbon of n-butane can contact the NP surface at the MOF/NP interface, while the composition of the NP surface—and consequently, its electronic structure—should be tuned so that only the desired sequence of reactions occurs on the contacting carbon. Identifying the ideal NP@MOF system, however, can be difficult due to the large number of possible MOF structures[17-20,40] and NP compositions[41]— not to mention the combinatorial explosion of their combinations. Therefore, insights obtained from DFT calculations can be highly valuable to begin to understand NP@MOF systems and help with their rational design.

One of the unusual aspects of utilizing NP@MOF systems for n-butane oxidation is that the catalysis would occur under steric constraints, creating a reaction scenario that has been largely unexplored for metal surfaces. Challenges in modelling n-butane oxidation (or other reactions) at the catalytically relevant NP/MOF interface include the computationally prohibitive large number of atoms involved in a fully atomistic model of the NP surface and MOF pores. Although this could be alleviated using QM/MM models,[42-45] these methods often require specialized codes and are not straightforward to use. In addition, the exact structure of the NP/MOF interface (which would change with the MOF) in these novel NP@MOF systems is not well characterized. To address these challenges, we propose a simple approach to explore – in a general way – the chemistry of metal catalyst surfaces under sterically constrained conditions using standard DFT programs.

In this approach we use a surrogate pore on top of a slab catalyst model to mimic the steric constraints that would arise from a given MOF pore. In this study, the surrogate pore is made of chemically inert atoms, whereas the slab is made of catalytically active palladium atoms. Note that this surrogate pore model focuses on steric effects and does not provide electrostatic interactions that may be important, for instance, in MOFs whose linkers have strongly polarized functional groups. Moreover, while the NP/MOF interface might include true NP/MOF chemical bonds that may alter the electronic structure of the NP, the surrogate pore model introduced here leaves the electronic structure of the metal surface essentially intact. The selection of palladium as the potential NP component was motivated by prior theoretical[46-49] and experimental[47,49-51] investigations of palladium and oxidized palladium for the oxidation of alkanes. After demonstrating the suitability of the surrogate pore to sterically constrain the interaction of reactants, intermediates and products on clean and oxygen-covered palladium surfaces, we sought to understand these interactions and their consequences on the reaction energies relevant to the catalytic oxidation of n-butane. Specifically, we focused on differences arising due to the presence or absence of the pore (i.e. presence or absence of steric constraints), the oxygen-coverage conditions, and the crystallographic structure of the palladium surface. We used this information as a first assessment of the potential suitability of Pd@MOF catalysts to regioselectively oxidize n-butane to 1-butanol.

Computational methods

Plane-wave density functional theory (PW-DFT) calculations were performed using the VASP code.[52-55] The electron exchange and correlation were described using the GGA Purdue-Burke-Ernzerhof (PBE)[56] functional, and core electrons were described using the projector-augmented wave method.[57,58] The D2 method of Grimme[59] was used to improve the modelling of dispersion interactions. An energy cutoff of 500 eV was used for Bloch waves to construct the solutions to the Kohn-Sham equations. All simulations used spin polarization. Gaussian smearing[60] was used to accelerate energy convergence with respect to the k-mesh density, but a smearing parameter of 0.03 was necessary to reduce T*S from the smearing to less than 0.001 eV/atom. Based on test runs, the electronic structure of a given geometry was considered solved when the energy difference between consecutive, self-consistent electronic steps was less than 10^{-5} eV. A geometry optimization was considered complete when the energy difference between consecutive geometries was less than 10^{-4} eV/atom. With these parameters, the maximum forces in an optimized geometry were in general smaller than 10^{-2} eV/Å.

The optimal lattice constant of bulk fcc palladium was calculated to be 3.959 Å, which is within 2% of the experimental value of 3.889 Å.[61] These calculations used a Gamma-centred 12x12x12 k-point mesh (energy converged within 10^{-3} eV/atom). From the DFT-optimized palladium fcc unit cell, we constructed 4-layered slabs of the Pd(111) and Pd(100) surfaces using the Surface Builder module of Materials Studio.[62] Both Pd(111) and Pd(100) were represented by a 4x4x1 simulation supercell, which was large enough to accommodate the surrogate pore. The simulation supercell included a 15 Å vacuum space between slabs along the z direction. The Crystal Builder module of Materials Studio[62] was used to place the pore and construct the simulation models in general. In all slab calculations, the supercell, the surrogate pore, and the two bottommost layers remained fixed, and a 4x4x1 k-point mesh was used (energy converged within $5x10^{-3}$ eV/atom). In select optimized geometries, we used the tetrahedron smearing method with Blochl corrections to compute the electron density.[63] This electron density was used with the Bader electron density splitting formalism to obtain atomic charges[64,65] and/or used in an additional non-self-consistent calculation using an 8x8x1 k-point mesh to obtain the electronic density of states. Optimizations of gas phase molecules and other isolated chemical species were done at the Γ point using a 15 Å x 15 Å x 20 Å orthogonal supercell.

Adsorption and interaction energies (E_{ads}) were calculated as follows. Note that we use the two terms interchangeably. A negative value of E_{ads} denotes a favourable interaction. The interaction energy of a chemical species "x" with a palladium surface *without* the pore is calculated in standard fashion as

$$E_{ads} = E_{slab+x} - E_{slab} - E_x \qquad (1)$$

where the three right-hand terms correspond to the total energies of the "slab + x" system and the slab and species x on their own. Similarly, for the interaction energy of chemical species "x" on the palladium surfaces *with* the pore we use
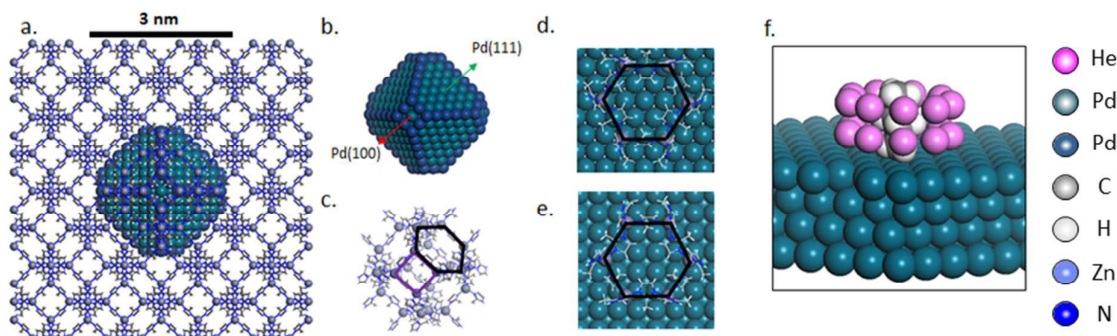
Fig 1. a) An all-atom model of a 3 nm truncated octahedral palladium nanoparticle (NP) encapsulated by a ZIF-8 porous shell: NP@ZIF-8. b) The Pd nanoparticle (d = 3 nm, 640 atoms) used in the molecular model in panel *a*. "Edge" atoms are coloured darker to help illustrate the NP shape and the boundaries of the NP facets. c) The sodalite cavity (d = 11.4 Å) that constitutes the ZIF-8 structure. The windows of the cavity are outlined in black and purple. d)-e) Possible ways that the ZIF-8 six-membered ring may contact the NP surface: d) Pd(111) and e) Pd(100). f) Perspective view of the artificial pore sterically constraining the adsorption of butane on Pd(111).

$$E_{ads} = E_{slab+pore+x} - E_{slab+pore} - E_x \qquad (2)$$

where the three right-hand terms correspond to the total energies of the "slab + pore + x" and "slab + pore" systems and species x on their own. Note that if species "x" refers to O, H, or OH, E_x corresponds to half the total energy of an isolated oxygen, hydrogen, or hydrogen peroxide molecule, respectively. Also note that since we include oxygen-covered surfaces in our study, the "slab" term can also refer to an oxygen-covered surface.

To quantify the thermodynamic favourability of a given reaction we calculated reaction energies, E_{rxn}. If a reaction on the palladium surface slab *without* the pore involves the adsorbed species x*, y*, xy* so

$$x^* + y^* \rightarrow xy^* + * \qquad (3)$$

then the reaction energy is calculated as

$$E_{rxn} = E_{slab+xy} + E_{slab} - E_{slab+x} - E_{slab+y} \qquad (4)$$

where the right-hand terms are the total energies of the "slab + xy" (xy*), "slab" (*), "slab + x" (x*) and "slab + y" (y*) systems. Similarly, if reaction *3* occurs on the palladium surface slab with the pore, the reaction energy is calculated instead as

$$E_{rxn} = E_{slab+pore+xy} + E_{slab+pore} - E_{slab+pore+x} - E_{slab+pore+y} \qquad (5)$$

where the right-hand terms are the total energies of the "slab + pore + xy" (xy*), "slab + pore" (*), "slab + pore + x" (x*) and "slab + pore + y" (y*) systems. As with interactions energies, the "slab" term in eq. 4 and 5 can refer to clean or oxygen-covered surfaces

To understand the role of dispersion forces on interactions and reactions, we obtained a*pproximate* estimations of the contribution of dispersion interactions—modelled with the Grimme term—to adsorption and reaction energies by applying equations 1 through 5 using only the contributions of the Grimme term to the respective total energies instead of the total energies themselves.

Surrogate pore model

We illustrate the type of system that we aim to model in Figure 1a, which shows an all-atom model of a region of a NP@MOF composite. The figure shows a truncated octahedral palladium

nanoparticle surrounded by the porous structure of the prototypical zeolitic imidazolate framework (ZIF) **ZIF-8**.[66] In this MOF, 2-methylimidazole linkers connect Zn(II) ions to form a 4-connected network of sodalite (**sod**) topology. **ZIF-8** has often been used in NP@MOF composites[16,25,27,29] and demonstrated to engender regioselective catalysis, as previously mentioned.[25] Nanoparticle sizes that have been employed in **ZIF-8**-based composites have reached sizes up to 100 nm.[16] The model in Figure1a shows a 3 nm nanoparticle (Figure 1b), as used in several works.[25,30,31] A particle of this size cannot be embedded within a defect-free **ZIF-8** structure, because the **ZIF-8** cavities (Figure 1c) are less than 1.2 nm in diameter. Thus, conceptually, one can imagine that cavities of ~3 nm must be "carved" within the perfect **ZIF-8** crystal to host 3 nm nanoparticles. However, so far, the characterization of NP@MOF composites leaves the exact structure of the host cavities and the NP/MOF interface unknown.

ZIF-8 has two types of windows corresponding to four- and six-membered rings, which are outlined in purple and black, respectively, in Figure 1c. Only the six-membered ring is believed to allow the passage of molecules such as alkanes and alcohols from one cavity to another.[67-69] Based on the experimental evidence of regioselectivity in NP@**ZIF-8** composites, one can hypothesize that in some regions of the NP/**ZIF-8** interface there are six-membered rings on top of the nanoparticle facets such as Pd(111) (Figure 1d) and Pd(100) (Figure 1e).   The NP/**ZIF-8** interface is shown in Figure1d,e with the ZIF Zn(II) ions closest to the Pd surfaces, but whether the Zn(II) ions or the 2-methylimidazole linkers are closest to the metal surface is not known. However, what seems certain from catalysis experiments is that steric constraints on molecules *are* imposed by the MOF at the NP/MOF boundary.[25]

It is important to note that although the MOF plays a role by imposing steric constraints, it is the nanoparticle that ultimately brings the catalytic functionality to NP@MOF composites, and thus the nanoparticle structure and composition warrant careful analysis and design. On these grounds, we used a surrogate pore model (shown in Figure 1f sterically constraining the adsorption of n-butane on Pd(111)) that allows us to focus on the chemistry occurring on the surface of the sterically constrained catalyst. This pore is constructed here using chemically inert helium atoms, which with
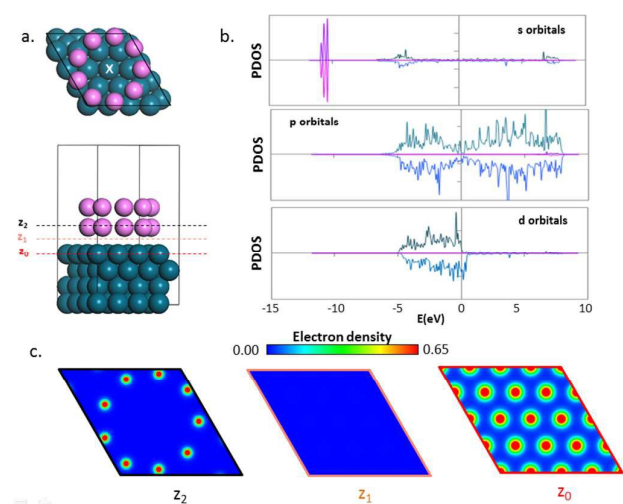
Fig. 2. a) Top and side views of the simulation supercell for the atop-centred surrogate pore on Pd(111). b) Contributions to the partial density of states of palladium (green and blue lines) and pore atoms (purple and pink lines) for the system in panel *a*. c) Electron density mapped on different horizontal slices cut at the heights indicated in panel *a*. Atoms coloured as in Fig.1.

only two valence electrons are expected to only moderately increase the computational costs of the DFT calculations. Note that the inert character of the surrogate pore is expected to chemically affect neither the catalyst surface nor the adsorbed species.

Results and discussion

Validation of the surrogate pore model

Surrogate pore geometric description. The surrogate pore was used on Pd(111) and Pd(100) surfaces centred at either a hollow or atop position. Figure 2a shows the simulation supercell for a Pd(111) surface with an atop-centred pore. The top and bottom rings of the surrogate pore are separated by 2.8 Å, and the bottom ring and topmost palladium layer are separated by 3.5 Å ($|z_2-z_0|$ in Figure 2a). These distances and all others reported on this work are based on center-to-center distances. Each pore ring is composed of nine helium atoms evenly distributed along the circumference of an 8.8 Å diameter circle (He-He distance equal to 3.0 Å). As a reference for the sizes of the surrogate pore atoms, note that $\sigma_{He} = 2.63$ Å.[70]

The goal of the pore design is to i) prevent repulsive interactions between pore atoms that would sharply increase the energy of the system, ii) minimize the number of atoms required to make the surrogate pore, iii) preclude any chemical species from being able to pass between pore atoms, iv) minimize effects of the surrogate pore on the electronic structure of the catalyst surface, and v) leave *all* surface sites available for the chemisorption of small chemical species, i.e. O, H, and OH. The following subsections show that the design goals were achieved.

Surrogate pore interaction with the catalyst. We determined whether the interaction between the surrogate pore and a palladium surface would affect the electronic structure of the latter through electronic structure analysis. Figure 2b shows the contribution of pore and catalyst atoms to the partial density of states (PDOS) for the system in Figure2a. Note that occupied
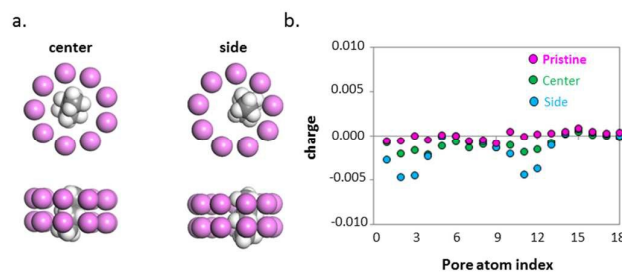

Fig. 3. a) n-butane interacting with the surrogate pore (no Pd surface) in two different configurations. b) Atomic charges of the pore atom in the absence (pristine pore) and in the presence of n-butane.

Table 1. Calculated interaction energies between the surrogate pore and the palladium surfaces. Values in parenthesis correspond to the van der Waals contribution to the interaction energies.

Metal surface	Pd/ring interaction [kJ/mol]	
	Hollow	Atop
Pd(100)	-17 (-13)	-17(-13)
Pd(111)	-19 (-19)	-20(-19)

Table 2. Calculated Interaction energies between the surrogate pore and n-butane. Values in parenthesis correspond to the van der Waals contribution to the interaction energies.

Pore packing	Interaction energy [kJ/mol]	
	Side	Center
Square	-9 (-9)	-6 (-5)
Triangular	-10 (-8)	-7 (-6)

(< 0 eV) energy levels corresponding to pore atoms (s-orbitals) are only found below -10 eV, whereas those corresponding to catalyst atoms are only found above -5 eV. This clear separation between pore and catalyst levels denotes the absence of any significant mixing of the electronic states of the surrogate pore and the catalyst surface. Similarly, Figure 2c shows a clear separation of the electron cloud of the palladium surface and the pore, as indicated by the virtual absence of electron density at the midpoint between these two ($z=z_1$). The above is reflected in the weak interaction energies calculated between the pore and Pd(100) and Pd(111) surfaces with hollow- and atop-centred pores (Table 1), which are essentially unaffected by the centring of the pore. Note that 76-95% of the interaction energy—depending on the surface— originates from the van der Waals term. The slightly stronger interactions of the pore with Pd(111) are likely due to the higher surface density of Pd(111) compared to Pd(100).

Surrogate pore interaction with molecules. Due to the tetragonal and trigonal shapes of the Pd(100) and Pd(111) supercells, respectively, the surrogate pores take on a different "packing" arrangement on each surface, i.e., square and triangular packing on Pd(100) and Pd(111), respectively (Figure S2). To analyse the pore/molecule interactions in the absence of the metal surface, we placed butane molecules inside the pore in the manner shown in Figure 3a, and calculated interaction energies (Table 2). The "side"

Table 3. O and H adsorption energies, E_{ads}, at different Pd(111) surface sites with and without the presence of the pore.

	Adsorption Energy (kJ/mol)			
	O w/ pore	O w/o pore	H w/ pore	H w/o pore
Hollow fcc	-134	-134	-63	-62
Hollow hcp	-115	-115	-56	-56
Bridge	-87	-87	-48	-47
Atop	6	6	-13	-13

Table 4. Comparison of select atomic charges with and without the pore for the systems shown in Figure 4b-d (O, H and OH adsorbates): charge of oxygen and hydrogen atoms, average charge of the (three) nearest palladium atoms to the adsorbate, charge of the pore (helium) atom nearest to the adsorbate.

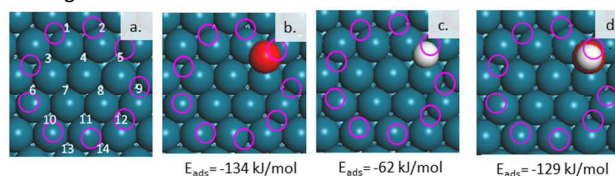|	O adsorption		H adsorption		OH adsorption	
	No pore	Pore	No pore	Pore	No pore	Pore
Oxygen	-0.675	-0.671	-	-	-1.079	-1.068
Hydrogen	-	-	-0.073	-0.087	0.642	0.626
Palladium	0.211	0.210	-0.016	0.002	0.130	0.134
Helium	-	-0.002	-	-0.002	-	-0.003

configuration has a slightly stronger interaction energy (-10 kJ/mol), with almost 90% corresponding to dispersion interactions (Table 2). This suggests no significant charge transfer or other electronic effects occurring during pore/butane interactions, as confirmed by Bader atomic charge analysis (Figure 3b). Note that the inclusion of butane in the pore only changes the charge of the pore atoms from (essentially) zero to -0.005 at most. With these calculations we show that the surrogate pore sterically constrains molecular species, such as n-butane, while remaining chemically inert.

Surrogate pore influence on surface accessibility. Our final test is to determine whether, as intended in the design of the pore, all catalyst sites can be accessed by small species such as O, H, and OH without impact on the adsorption energies. Table 3 shows that within 1 kJ/mol O and H adsorption on different surface sites was equal with and without the pore, and the adsorption trends agree with reported adsorption energies[71-75] and preferred adsorption sites observed experimentally.[76,77] O, H and OH accessibility to the catalyst surface in the presence of the pore was evaluated by adsorbing O, H and OH adsorption on fourteen Pd(111) hollow fcc sites (Figure 4a) with the pore present. Figure 4b-d shows O, H and OH adsorbed directly below a pore atom. Within a 1 kJ/mol tolerance, the adsorption energies of O, H, and OH on all sites were -134, -62 and -129 kJ/mol, respectively. Furthermore, Bader charge analysis shows that there are not significant differences in the atomic charges of a given adsorbate or between different surface sites independently of whether the pore is present (Table 4).

Exploration of n-butane oxidation

In the previous subsections we demonstrated that the only expected effect of the surrogate pore is to sterically constrain the adsorption of long molecular species such as n-butane in the manner that would occur in a suitable NP@MOF system. On the other hand, all surface sites remained accessible for small species

such as O, H and OH. We now proceed to use the surrogate pore to investigate

Fig. 4. a) Tested adsorption sites (1 through 14) for O, H and OH on Pd(111) with an atop-centred pore. b-d) Snapshots of O (b), H (c) and OH (d) adsorbed at site 5, and the corresponding adsorption energies.
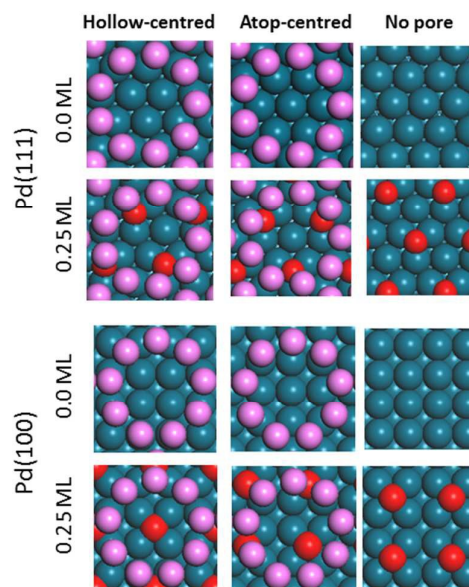
Fig. 5. Surface and pore/surface systems investigated in this work: Pd(111) or Pd(100) with a hollow-centred pore, an atop-centred pore, or no pore and with no oxygen coverage or 0.25 ML coverage of oxygen .

n-butane oxidation under sterically constrained conditions.

Catalyst conditions and reactions. Here we focus on the catalyst surfaces and coverages shown in Figure 5, which include the catalyst surface without the pore and with the hollow-centred and atop-centred pore. The centring of the pore was varied to see whether the exact location of the pore relative to the surface affects the adsorption energies and, in turn, the reaction energies. The atop- and hollow-centring were chosen because adsorption on atop and hollow sites are typically markedly different (Table 3). The "pore-free" surfaces were chosen to compare between sterically-constrained and unconstrained n-butane oxidation. Clean and oxygen-covered Pd(111) and Pd(100) surfaces were studied. Oxygen-covered surfaces were included because pre-adsorbed oxygen has been shown to affect reactions in other oxidation systems,[49,78,79] although here we only considered moderate oxygen coverages (0.25 ML). At this coverage both Pd(111) and Pd(100) present a 4 to 1 Pd to O ratio at the surface, making them suitable for direct comparison. This comparison is not possible at higher oxygen coverages because, as also reported experimentally,[80] higher oxygen content leads to the deformation of Pd(100), which hints to the susceptibility of palladium to oxidize to palladium oxide via this facet.[81-83]
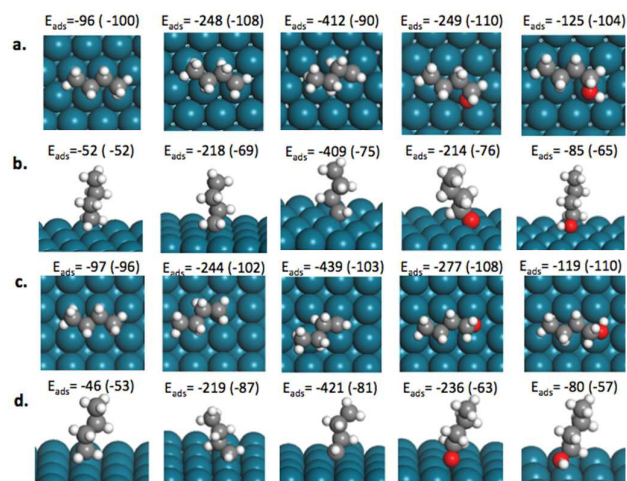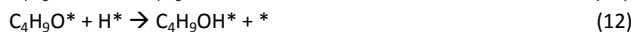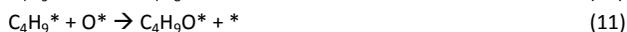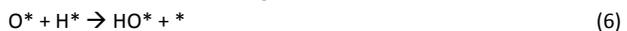
Fig. 6. Most favourable adsorption (interaction) configurations of (from left to right) n-butane (C_4H_{10}), 1-butyl (C_4H_9), 1-butenyl (C_4H_8), 1-butoxy (C_4H_9O), and 1-butanol (C_4H_9OH) on a) Pd(111) with no pore, b) Pd(111) with the atop-centred pore, c) Pd(100) with no pore, and d) Pd(100) with the atop-centred pore. Adsorption (interaction) energies, E_{ads}, are given in kJ/mol and calculated using eq.1 (*a* and *c*) or eq. 2 (*b* and *d*). Values in parentheses are estimates of the contribution of dispersion interactions to the adsorption energies. Pore atoms in *b* and *d* are not shown for clarity.

We focus on the following reactions

$$O* + H* \rightarrow HO* + * \tag{6}$$
$$C_4H_{10}* + * \rightarrow C_4H_9* + H* \tag{7}$$
$$C_4H_{10}* + O* \rightarrow C_4H_9* + HO* \tag{8}$$
$$C_4H_9* + * \rightarrow C_4H_8* + H* \tag{9}$$
$$C_4H_9* + O* \rightarrow C_4H_8* + HO* \tag{10}$$
$$C_4H_9* + O* \rightarrow C_4H_9O* + * \tag{11}$$
$$C_4H_9O* + H* \rightarrow C_4H_9OH* + * \tag{12}$$
$$C_4H_9O* + OH* \rightarrow C_4H_9OH* + O* \tag{13}$$

where the C_4 species correspond to n-butane (C_4H_{10}), 1-butyl or 2-butyl (C_4H_9), 1-butenyl or 2-butenyl (C_4H_8), 1-butoxy or 2-butoxy (C_4H_9O), and 1-butanol or 2-butanol (C_4H_9OH). We postulate that a possible route for 1-butanol formation is the sequence n-butane→1-butyl → 1-butoxy→1-butanol (i.e. reaction 7 (or 8) → reaction 11 → reaction 12 (or 13)), and here we calculate whether that sequence is thermodynamically favoured in any of the systems studied instead of the sequence n-butane→1-butyl→1-butenyl (i.e. reaction 7 (or 8) → reaction 9 (or 10)), which leads to further dehydrogenated products. Note that without the pore, the "n-butane→2-butyl→2-butoxy→2-butanol" and "n-butane→2-butyl→2-butenyl" sequences are also possible and are, thus, explored.

Adsorption of C_4 species. We first calculated the most stable adsorption configurations and energies of all species mentioned above to understand their interactions with the palladium surfaces with and without pre-adsorbed oxygen and with and without steric constraints. The most stable adsorption configurations and corresponding adsorption energies are shown in Figure 6 (clean palladium) and Figure 7 (oxygen-covered palladium) for the linear ("1-") C_4 species without and with the atop-centred pore (detailed adsorption configuration for all species on all systems are shown in

Table 5. Calculated adsorption energies in kJ/mol for different C_4 species on Pd(111) and Pd(100) surfaces without oxygen coverage.

Species	No pore		Atop-centred pore		Hollow-centred	
	Pd(111)	Pd(100)	Pd(111)	Pd(100)	Pd(111)	Pd(100)
n-butane	-96	-97	-52	-46	-55	-56
1-butyl	-248	-244	-218	-219	-215	-229
2-butyl	-229	-237	-	-	-	-
1-butenyl	-424	-439	-409	-421	-410	-423
2-butenyl	-412	-430	-	-	-	-
1-butoxy	-249	-277	-214	-236	-216	-241
2-butoxy	-260	-273	-	-	-	-
1-butanol	-126	-119	-85	-80	-90	-89
2-butanol	-123	-128	-	-	-	-

Figures S5-S10). Table 5 and Table 6 additionally show adsorption energies for all C_4 species (including the "2-" C_4 species on pore-free surfaces[84]). Without the pore, n-butane adsorbs horizontally on all surfaces with all carbons at a ~2.9 Å distance from the topmost Pd layer. This agrees with other computational reports of n-butane adsorption on metallic (111) and (100) surfaces.[85,86] n-butane adsorption energy magnitudes are higher on clean surfaces (96-97 kJ/mol) than on oxygen-covered surfaces (73-88 kJ/mol). With the pore, n-butane sits roughly perpendicular to the surface with the closest carbon to the topmost Pd layer at a distance of ~2.9 Å. Note that while the interaction of n-butane with the pore is favourable (Table 2), the reduction of contact points between the vertically adsorbed n-butane and the palladium surfaces weakens the adsorption energy by 17 to 51 kJ/mol depending on surface conditions. With and without the pore, if there is pre-adsorbed oxygen, n-butane orients so it interacts with Pd atoms instead of O atoms (Figure 7 and Figure S5). Also note that with or without the pore, n-butane adsorption is dominated by dispersion interactions (Figure 6).

The adsorption of dehydrogenated C_4 radicals, on the other hand, is dominated by chemical bonding. Although 1- and 2-butyl adsorption tends to be weaker on oxygen-covered surfaces than on clean surfaces, in all surface conditions (with and without the pore) the adsorption energy magnitudes are higher than 200 kJ/mol, with dispersion interactions contributing less than 50%. In all cases, the butyl radicals adsorb by placing the dehydrogenated carbon at a top position to form one 2.0 Å Pd-C bond. Without the pore, the butyl radicals adsorb in horizontal fashion, although bending slightly to allow the formation of the Pd-C bond. As with n-butane, if there is pre-adsorbed oxygen, the butyl radical orients so all parts of the radical interact with Pd instead of O (Figure 7 and Figure S6). With the pore, 1-butyl is much less perpendicular to the surface than n-butane to ensure the formation of the Pd-C bond (Figure S6). As a result of the vertical adsorption, the adsorption energy of 1-butyl is weakened by ~14-31 kJ/mol depending on the surface conditions and pore centring. In general this is a less marked weakening than for n-butane, probably due to the more significant role of dispersion interactions on n-butane than 1-butyl.
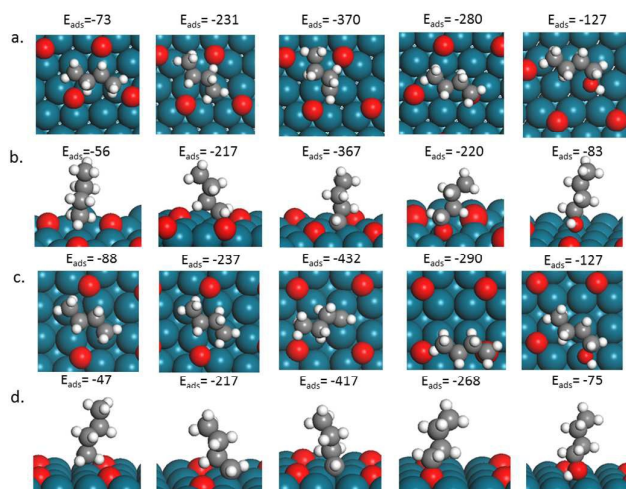

Fig. 7. Most favourable adsorption (interaction) configurations of (from left to right) n-butane (C_4H_{10}), 1-butyl (C_4H_9), 1-butenyl (C_4H_8), 1-butoxy (C_4H_9O), and 1-butanol (C_4H_9OH) on a) 0.25 ML O@Pd(111) with no pore, b) 0.25 ML O@Pd(111) with the atop-centred pore, c) 0.25 ML O@Pd(100) with no pore, and d) 0.25 ML O Pd(100) with the atop-centred pore. Adsorption (interaction) energies, E_{ads}, are given in kJ/mol. Pore atoms in *b* and *d* are not shown for clarity.

Table 6. Calculated adsorption energies in kJ/mol for different C_4 species on Pd(111) and Pd(100) surfaces with oxygen coverage.

Species	No pore		Atop-centred pore		Hollow-centred	
	Pd(111)	Pd(100)	Pd(111)	Pd(100)	Pd(111)	Pd(100)
butane	-73	-88	-56	-47	-55	-41
1-butyl	-231	-237	-217	-217	-215	-206
2-butyl	-217	-222	-	-	-	-
1-butenyl	-370	-432	-367	-417	-370	-391‡
2-butenyl	-382	-414	-	-	-	-
1-butoxy	-280	-290	-220	-268	-221	-257
2-butoxy	-296	-298	-	-	-	-
1-butanol	-127	-127	-83	-75	-88	-86
2-butanol	-131	-125	-	-	-	-

Dispersion interactions have even less contribution (less than 25%) in the adsorption of 1- and 2-butenyl. The butenyl radicals adsorb by placing the dehydrogenated carbon on a bridge position forming two 2.0 Å Pd-C bonds, which primarily account for the adsorption energy (magnitudes higher than 350 kJ/mol). Without the pore, the butenyl radicals adsorb horizontally, but with the pore n-butenyl sits roughly perpendicular to the surface; less so than n-butane, but more so than n-butyl (Figure S9). However, perhaps due to the relatively smaller role of dispersion interactions in 1-butenyl adsorption, the differences in adsorption energies with and without the pore are only in the 3-18 kJ/mol range[87] depending on the surface conditions. In fact, surface conditions seem to have a bigger impact on the adsorption of 1-butenyl radicals than whether the pore is present. For instance, on Pd(111), the pre-adsorbed oxygen weakens the adsorption of 1-butenyl by more than 40 kJ/mol (Figure S12) with and without the pore, and it also accentuates differences between 1-butenyl adsorption of Pd(111) and Pd(100) (>60 kJ/mol), which are not so pronounced on the clean surfaces (< 25 kJ/mol) (Figure S15).

In general, the way the dehydrogenated carbons of butyl and butenyl radicals coordinate to surface palladium atoms agrees with the coordination of C_1 radicals reported in DFT studies of methane dehydrogenation on palladium.[46,48] Trends in interaction energies agree as well, with Trinchero *et al.,*[48] for instance, reporting a -167 kJ/mol adsorption energy for the CH_3 radical and -399 kJ/ml for the CH_2 radical.

The oxygenated species 1- and 2-butoxy adsorb on clean surfaces by placing their oxygen atom either at a bridge position forming two 2.1 Å Pd-O bonds (for clean surfaces) or at a hollow position forming three longer Pd-O bonds (for oxygen-covered surfaces). However, in light of the adsorption energy magnitudes (<300 kJ/mol), these bonds are not as strong as the Pd-C bonds formed

during the adsorption of butenyl radicals. Therefore, the relative contribution of dispersion interactions to the adsorption energy is higher for 1- and 2-butoxy than for the butenyl radicals, and differences in adsorption strengths with and without the pore are also higher for the former (Figure S13). As with previous species, without the pore, 1- and 2-butoxy adsorb horizontally, whereas with the pore n-butoxy sits roughly perpendicular, although less so than any of the other C_4 species (Figure S7). For butoxy adsorption on O-covered surfaces (Figure 7), the butoxy oxygen is assumed to have come from one of the surface oxygens from the configurations in Figure 5. Thus if 1- or 2-butoxy desorbs, the surface is left with one oxygen "vacancy." We use the surfaces with vacancies to calculate the adsorption energy of butoxy on O-covered surfaces. According to our calculations, the adsorption energy of 1- and 2-butoxy is higher in magnitude on the oxygen-covered surfaces than on the clean surfaces. Also, when there is pre-adsorbed oxygen, 1- and 2-butoxy orient to interact with Pd atoms instead of O atoms.

The adsorption energies of 1- and 2-butanol are calculated in a similar fashion as for 1- and 2- butoxy. However, the adsorption of 1- and 2-butanol is more similar to that of n-butane, although somewhat stronger. Dispersion interactions dominate the adsorption, which occurs horizontally and vertically without and with the pore, respectively, leading to a weakening of the adsorption energy by 30-52 kJ/mol depending on the surface coverage. In general, 1- and 2-butanol adsorb with the hydroxyl oxygen (almost) atop of a palladium atom with a ~2.4 Å Pd-O distance (Figure 6, Figure 7 and Figure S10). Similar to n-butane, differences in adsorption energies on Pd(111) and Pd(100) are minimal.

Interestingly, the position of the pore on the surface does not seem to affect the interaction energy of C_4 species as much as we had anticipated. Indeed, the largest differences in interaction energies between atop-centred and hollow-centred pores were 5 kJ/mol on Pd(111) and 10 kJ/mol on Pd(100) (Figure S14).[87] Thus, for clarity, from this point on we will focus our discussion only on the atop-centred pore.
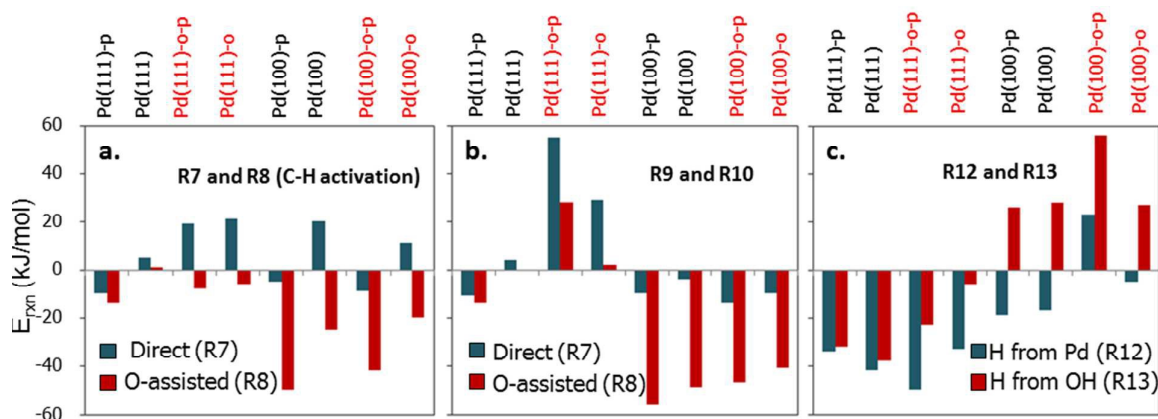
Fig. 8. Reaction energies for different catalyst surfaces and conditions for a) C-H activation (n-butane → 1-butyl; reactions 7 and 8), b) Second dehydrogenation (1-butyl → 1-butenyl; reactions 9 and 10), and c) 1-butoxy hydrogenation (1-butoxy → 1-butanol; reactions 12 and 13). Suffix "-p" added for surfaces with the atop-centred pore, "-o" added for 0.25 ML oxygen-covered surfaces.
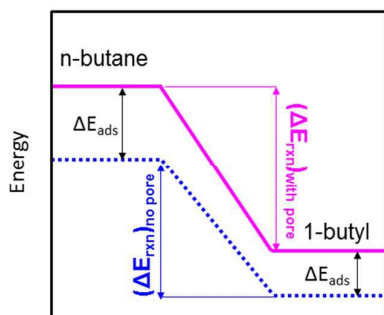

Fig. 9. Generalized schematic of how steric constraints from the pore increase the favourability of C-H activation by weakening n-butane adsorption relative to 1-butyl adsorption. ΔE_{ads} indicates the change in adsorption energy upon adding the pore. The dashed line indicates energies without the pore, and the solid line indicates energies with the pore.

Implications of adsorption strengths on reaction energies. With the energies for the lowest-energy adsorption configurations on the clean and oxygen-covered surfaces, we calculated the reaction energies for reactions 6 through 13 using Equations 4 and 5 (all reaction energies are reported in Table S2). We find that reaction 6 is unaffected by the presence of the pore and more favourable on Pd(100) than on Pd(111). Combining adsorbed H and O to form OH is exothermic only by 4 kJ/mol on clean Pd(111), but by 46 kJ/mol on clean Pd(100). This marked difference is reduced, however, with oxygen coverage where hydroxyl formation is exothermic by 28 kJ/mol on Pd(111) and by 33 kJ/mol on Pd(100) when they have 0.25 ML of pre-adsorbed oxygen. Since hydroxyl formation is favourable for all studied surfaces and conditions, the activation of the primary C-H bond of n-butane is more favourable when it is O-assisted (reaction 8) than when it is direct (reaction 7) (Figure 8a). This favourability is slight on clean§ Pd(111) and more pronounced for all other cases.

Notably, whether O-assisted or direct, C-H activation is more favourable in the presence of the pore (compare the surface and surface-p cases in Figure 8a). Since H adsorption and hydroxyl formation are unaffected by the pore, the changes in favourability must arise from the effects of the pore on n-butane and 1-butyl adsorption. Recall from the previous subsection that weakening of n-butane adsorption is more pronounced upon adding the pore than the corresponding weakening for 1-butyl adsorption.

Therefore, although palladium or pre-adsorbed oxygen binds the hydrogen extracted from the n-butane equally strong with and without the pore, it is relatively more favourable to have 1-butyl adsorbed than n-butane when the pore is present (Figure 9). The favourability of C-H activation due to the pore, however, is less marked for Pd(111) when there is pre-adsorbed oxygen ("Pd(111)-o-p" vs. "Pd(111)-o" in Figure 8a).

The second dehydrogenation of the activated carbon of 1-butyl (reactions 9 and 10) is also more favourable O-assisted than direct and also significantly more favoured on Pd(100) than on Pd(111) at any surface conditions (Figure 8b). When the surfaces are clean (blue bars), this is primarily due to Pd(100) being more favourable than Pd(111) toward hydroxyl formation; when the surfaces have pre-adsorbed oxygen (red bars) this is primarily due to Pd(100) binding more strongly than Pd(111) 1-butyl and 1-butenyl. Remarkably, with the pore, the second dehydrogenation seems to be relatively unfavourable (>20 kJ/mol endothermic) for Pd(111) with 0.25 ML oxygen coverage ("Pd(111)-o-p" in Figure 8b), mainly due to the considerable weakening of 1-butenyl adsorption caused by the pre-adsorbed oxygen.

As shown in Figure 8c, at all surface conditions, hydrogenating 1-butoxy to form 1-butanol through reaction 13 is less favourable on Pd(100) (endothermic) than on Pd(111) (exothermic). This is partly due to (again) the favourability of Pd(100) to form hydroxyls—which makes it less favourable to break the adsorbed OH to transfer the H to 1-butoxy—and partly due to the stronger adsorption of butoxy on Pd(100) than Pd(111). The hydrogenation of 1-butoxy to 1-butanol is only slightly affected by the presence of the pore when the surfaces are clean. However, when there is pre-adsorbed oxygen the pore makes the reaction even less favourable on Pd(100) ("Pd(100)-o-p" versus "Pd(100)-o" in Figure 8c), but notably it makes it more favourable on Pd(111) ("Pd(111)-o-p" versus "Pd(111)-o" in Figure 8c).

The formation of 1-butoxy (reaction 11) is exothermic in all cases except for Pd(111) when the pore is present, in which the reaction is slightly endothermic (10 kJ/mol) (Figure 10 red bars). Comparing the red and gray bars in Figure 10, we see that in most cases the reaction energies are similar or lower (more favourable) for 1-butenyl formation (O-assisted) compared to 1-butoxy formation. Notably the exception is Pd(111) with 0.25 ML oxygen coverage, in

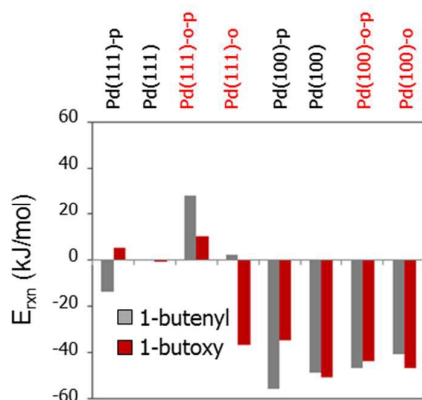which case the 1-butoxy formation is clearly favoured over that of 1-butenyl.

Fig. 10. Comparison of reactions energies for the O-assisted second dehydrogenation (reaction 10) and for the formation of 1-butoxy (reaction 11) for different catalyst surfaces and conditions. Suffix "-p" added for surfaces with the pore, "-o" added for 0.25 ML oxygen-covered surfaces.

Without the pore, reactions on the secondary carbon of n-butane can also occur, and thus we also calculated the corresponding reaction energies (Table S2). Briefly, the trends discussed so far for the reactions on the primary carbon are also applicable for those on the secondary carbon (Figure S16), only that the reactions leading to the formation of 2-butoxy are overall slightly more favourable than those leading to 1-butoxy. However, the hydrogenation of 1-butoxy to 1-butanol is somewhat more favourable than that of 2-butoxy to 2-butanol, except on the case of clean Pd(100). Thus, without the pore, the overall sequence of reaction energies indicates that 2-butanol is equally or more favoured than 1-butanol on palladium.

With the pore, one promising system favouring 1-butoxy formation over 1-butenyl is Pd(111) with 0.25 ML oxygen coverage. Therefore, in Figure 11b we illustrate the complete set of reactions for this system. Figure 11 also shows some analogous systems for comparison purposes. (Note that the energies shown are the reaction energies and not reaction barriers. Searching for transition states and determining reaction barriers are planned for the future.) In "Pd(111)-o" (without pore; Figure 11a), activation of the secondary carbon is slightly more facile than the primary one (–9 versus –6 kJ/mol). For either butyl radical, the second dehydrogenation is slightly endothermic, because as previously noted O-coverage weakens the adsorption of butenyl radicals. Butoxy formation is thus preferred, although with the formation of 2-butoxy being more favourable than the formation of 1-butoxy (–62 versus –37 kJ/mol), 2-butanol formation may be favoured overall. On "Pd(100)-o" (without pore; Figure 11c), 2-butanol formation may also be favoured. Note, however, that both the C-H activation and second dehydrogenation are more favourable than for "Pd(111)-o", even if butoxy formation is still preferred to the second dehydrogenation. Also note that the (1- or 2-)butoxy conversion to (1- or 2-butanol) is less favourable than for "Pd(111)-o".

For "Pd(111)-o-p" (with pore; Figure 11b) the combination of oxygen coverage (making reaction 11 more favourable than reaction 10) and the presence of the pore (making reactions on the secondary carbon not possible) favours the targeted sequence of

reactions (with only one slightly endothermic step) that could form the desired 1-butanol. Note that the presence of the pore is a necessary but not sufficient condition to make the targeted
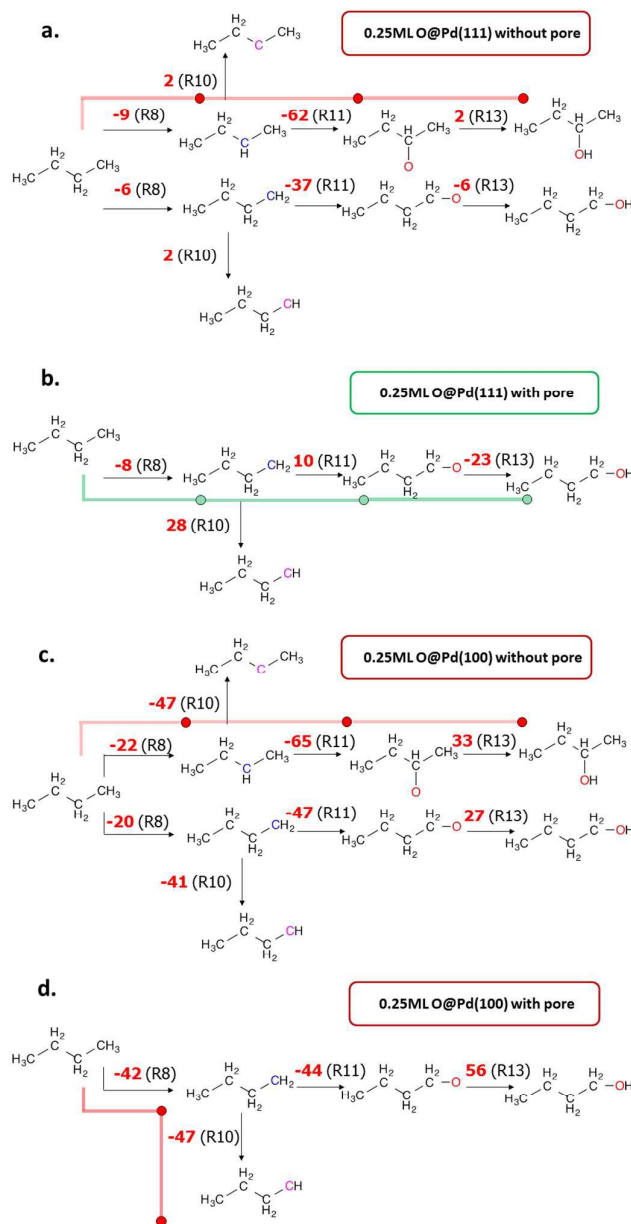

Fig. 11. Reaction energies on a) Pd(111) with 0.25 ML oxygen coverage and without the pore, b) Pd(111) with a 0.25 ML oxygen coverage and with the pore, c) Pd(100) with 0.25 ML oxygen coverage and without the pore, and d) Pd(100) with 0.25 ML oxygen coverage and with the pore. All reaction energies are in kJ/mol. The reaction numbers are in parentheses. The coloured lines indicate the favoured path according to the reaction energies.

sequence of reactions favourable. Consider the analogous system "Pd(100)-o-p" (with pore; Figure 11d) where although the reactions on the secondary carbon are eliminated, the formation of 1-butenyl is slightly favoured over the formation of 1-butoxy. Furthermore, note that if 1-butoxy is formed, its hydrogenation to 1-butanol in this case is endothermic by 56 kJ/mol.

We should note that the surface conditions studied here correspond to relatively low oxygen coverage, which as previously mentioned was done to facilitate comparison of the behaviour of the Pd(111) and Pd(100) facets. However, we also performed additional calculations on Pd(111) saturated with oxygen, i.e. 1 ML, which is a coverage unrealized on single crystal flat surfaces, but possible on nanoparticles.[49] With no available metal sites, all C_4 species adsorb on O atoms, and only O-assisted dehydrogenation is possible. This dehydrogenation is highly exothermic on both the primary carbon (-242 kJ/mol with the pore, -227 kJ/mol without the pore) and secondary carbon (-249 kJ/mol without the pore) forming directly 1-butoxy or 2-butoxy. However, the issue is that the dehydrogenation of the 1- or 2-butoxy is also exothermic by more than 200 kJ/mol, and thus significantly more favourable than the hydrogenation to form 1- or 2-butanol (less than 50 kJ/mol exothermic). Therefore, based on all tested conditions, palladium nanoparticles exposing (111) facets with moderate oxygen coverage (0.25 ML) and steric constraints provided by a suitable MOF shell may be a promising candidate for the selective oxidation of n-butane to 1-butanol.

Conclusions

We introduced a simple DFT modelling approach for MOF-encapsulated metal catalysts (NP@MOFs), where a surrogate pore composed of chemically inert atoms mimics the steric constraints imposed by the MOF. The surrogate pore is composed of inert helium atoms, which were chosen for computational efficiency. Different tests showed that the only expected effect of the pore is to sterically constrain the adsorption of C_4 species on the studied palladium surfaces. We carried out DFT calculations of the adsorption of species relevant to n-butane oxidation on different surfaces and conditions to discern the effects of surface structure, oxygen coverage, and the presence or absence of steric constraints. We showed that steric constraints cause the C_4 species to adsorb roughly perpendicular to the surface, weakening the adsorption compared to their horizontal configurations when there are no steric constraints. Overall, the weakening was more pronounced for n-butane and 1-butanol, whose adsorption is dominated by dispersion interactions, and less pronounced for 1-butyl, 1-butenyl, and 1-butoxy, whose adsorption is dominated by chemical interactions. Also we found that oxygen coverage tended to weaken the adsorption of the oxygen-free C_4 species and strengthen the adsorption of oxygen-containing C_4 species.

Based on calculated reaction energies, we showed that the activation of the primary n-butane C-H bond was more favourable when assisted by O than when catalysed directly by the Pd surface, and more favourable on Pd(100) than on Pd(111), partly due to higher favourability of hydroxyl formation on the former surface. This, however, also makes the hydrogenation of 1-butoxy less favourable on Pd(100). We also showed that the presence of the pore increases the favourability of C-H activation by weakening n-butane adsorption relative to 1-butyl adsorption. In most palladium systems, further dehydrogenation of 1-butyl is equally or more favourable than 1-butoxy formation, with the exception of Pd(111) with 0.25 ML oxygen-coverage. This was shown to be due to the weakening of n-butenyl adsorption due to the presence of pre-adsorbed oxygen. If this effect on Pd(111) is combined with the imposition of steric constraints, the targeted sequence of reactions to produce 1-butanol is favoured. This result may provide a design

for NP@MOF catalysts for selective oxidation of normal alkanes to primary alcohols. Future work will include the calculation of kinetic energy barriers using the pore modelling approach demonstrated here and microkinetic modelling for catalytic surfaces such as palladium and palladium alloys.

Notes

‡ The large difference (26 kJ/mol) of n-butenyl adsorption on 0.25 ML oxygen-covered Pd(100) depending on whether the pore is atop-centred or hollow-centred arose because for the latter one of the pre-adsorbed oxygen atoms moved out of its original position.
§ We use the term "clean" surface although one pre-adsorbed oxygen needs to be present to carry out reactions 6, 8, and 10, 11 and 13. One pre-adsorbed oxygen on a 4x4 supercell corresponds to a 0.0625 ML oxygen coverage.

References

(1) Anastas, P. T.; Kirchhoff, M. M. Origins, Current Status, and Future Challenges of Green Chemistry *Acc. Chem. Res.* **2002**, *35*, 686-694.

(2) Arndtsen, B. A.; Bergman, R. G.; Mobley, T. A.; Peterson, T. H. Selective Intermolecular Carbon-Hydrogen Bond Activation by Synthetic Metal Complexes in Homogeneous Solution *Acc. Chem. Res.* **1995**, *28*, 154-162.

(3) Guo, Z.; Liu, B.; Zhang, Q.; Deng, W.; Wang, Y.; Yang, Y. Recent Advances in Heterogeneous Selective Oxidation Catalysis for Sustainable Chemistry *Chem. Soc. Rev.* **2014**, *43*, 3480-3524.

(4) Linic, S.; Jankowiak, J.; Barteau, M. A. Selectivity Driven Design of Bimetallic Ethylene Epoxidation Catalysts From first Principles *J. Catal.* **2004**, *224*, 489-493.

(5) Rankin, R. B.; Greeley, J. Trends in Selective Hydrogen Peroxide Production on Transition Metal Surfaces from First Principles *ACS Catal.* **2012**, *2*, 2664-2672.

(6) Hirasawa, S.; Watanabe, H.; Kizuka, T.; Nakagawa, Y.; Tomishige, K. Performance, Structure and Mechanism of Pd–Ag Alloy Catalyst for Selective Oxidation of Glycerol to Dihydroxyacetone *J. Catal.* **2013**, *300*, 205-216.

(7) Wang, H.; Wang, C.; Yan, H.; Yi, H.; Lu, J. Precisely-Controlled Synthesis of Au@Pd Core–Shell Bimetallic Catalyst Via Atomic Layer Deposition for Selective Oxidation of Benzyl Alcohol *J. Catal.* **2015**, *324*, 59-68.

(8) Qin, Y.-l.; Liu, Y.-c.; Liang, F.; Wang, L.-m. Preparation of Pd–Co-Based Nanocatalysts and Their Superior Applications in

Formic Acid Decomposition and Methanol Oxidation *ChemSusChem* **2015**, *8*, 260-263.

(9)O'Neill, B. J.; Jackson, D. H. K.; Lee, J.; Canlas, C.; Stair, P. C.; Marshall, C. L.; Elam, J. W.; Kuech, T. F.; Dumesic, J. A.; Huber, G. W. Catalyst Design with Atomic Layer Deposition *ACS Catal.* **2015**, *5*, 1804-1825.

(10)Greeley, J.; Mavrikakis, M. Alloy Catalysts Designed from First Principles *Nat. Mater.* **2004**, *3*, 810-815.

(11)Norskov, J. K.; Bligaard, T.; Rossmeisl, J.; Christensen, C. H. Towards the Computational Design of Solid Catalysts *Nat. Chem.* **2009**, *1*, 37-46.

(12)Cao, H.; Pauff, J. M.; Hille, R. Substrate Orientation and Catalytic Specificity in the Action of Xanthine Oxidase: The Sequential Hydroxylation of Hypoxanthine to Uric Acid *J. Bio. Chem.* **2010**, *285*, 28044-28053.

(13)Ikeda, S.; Ishino, S.; Harada, T.; Okamoto, N.; Sakata, T.; Mori, H.; Kuwabata, S.; Torimoto, T.; Matsumura, M. Ligand-Free Platinum Nanoparticles Encapsulated in a Hollow Porous Carbon Shell as a Highly Active Heterogeneous Hydrogenation Catalyst *Angew. Chem.* **2006**, *118*, 7221-7224.

(14)Ge, J.; Zhang, Q.; Zhang, T.; Yin, Y. Core–Satellite Nanocomposite Catalysts Protected by a Porous Silica Shell: Controllable Reactivity, High Stability, and Magnetic Recyclability *Angew. Chem. Int. Ed.* **2008**, *47*, 8924-8928.

(15)Canlas, C. P.; Lu, J.; Ray, N. A.; Grosso-Giordano, N. A.; Lee, S.; Elam, J. W.; Winans, R. E.; Van Duyne, R. P.; Stair, P. C.; Notestein, J. M. Shape-Selective Sieving Layers on an Oxide Catalyst Surface *Nat. Chem.* **2012**, *4*, 1030-1036.

(16)Lu, G.; Li, S.; Guo, Z.; Farha, O. K.; Hauser, B. G.; Qi, X.; Wang, Y.; Wang, X.; Han, S.; Liu, X.; DuChene, J. S.; Zhang, H.; Zhang, Q.; Chen, X.; Ma, J.; Loo, S. C. J.; Wei, W. D.; Yang, Y.; Hupp, J. T.; Huo, F. Imparting Functionality to a Metal–Organic Framework Material by Controlled Nanoparticle Encapsulation *Nat. Chem.* **2012**, *4*, 310-316.

(17)Wilmer, C. E.; Leaf, M.; Lee, C. Y.; Farha, O. K.; Hauser, B. G.; Hupp, J. T.; Snurr, R. Q. Large-Scale Screening of Hypothetical Metal-Organic Frameworks *Nat. Chem.* **2012**, *4*, 83-89.

(18)Martin, R. L.; Lin, L.-C.; Jariwala, K.; Smit, B.; Haranczyk, M. Mail-Order Metal–Organic Frameworks (MOFs): Designing Isoreticular MOF-5 Analogues Comprising Commercially Available Organic Molecules *J. Phys. Chem. C* **2013**, *117*, 12159-12167.

(19)Gomez-Gualdron, D. A.; Gutov, O. V.; Krungleviciute, V.; Borah, B.; Mondloch, J. E.; Hupp, J. T.; Yildirim, T.; Farha, O. K.; Snurr, R. Q. Computational Design of Metal–Organic Frameworks Based on Stable Zirconium Building Units for Storage and Delivery of Methane *Chem. Mat.* **2014**, *26*, 5632-5639.

(20)Bao, Y.; Martin, R. L.; Simon, C. M.; Haranczyk, M.; Smit, B.; Deem, M. W. In Silico Discovery of High Deliverable Capacity Metal–Organic Frameworks *J. Phys. Chem. C* **2015**, *119*, 186-195.

(21)Mason, J. A.; Veenstra, M.; Long, J. R. Evaluating Metal-Organic Frameworks for Natural Gas Storage *Chem. Sci.* **2014**, *5*, 32-51.

(22)Zhao, D.; Yuan, D.; Zhou, H.-C. The Current Status of Hydrogen Storage in Metal-Organic Frameworks *Energy. Environ. Sci.* **2008**, *1*, 222-235.

(23)Snurr, R. Q.; Hupp, J. T.; Nguyen, S. T. Prospects for Nanoporous Metal-Organic Materials in Advanced Separations Processes *AIChE J.* **2004**, *50*, 1090-1095.

(24)Lee, J.; Farha, O. K.; Roberts, J.; Scheidt, K. A.; Nguyen, S. T.; Hupp, J. T. Metal-Organic Framework Materials as Catalysts *Chem. Soc. Rev.* **2009**, *38*, 1450-1459.

(25)Stephenson, C. J.; Hupp, J. T.; Farha, O. K. Pt@Zif-8 Composite for the Regioselective Hydrogenation of Terminal Unsaturations in 1,3-Dienes and Alkynes *Inorg. Chem. Front.* **2015**, *2*, 448-452.

(26)Aijaz, A.; Karkamkar, A.; Choi, Y. J.; Tsumori, N.; Rönnebro, E.; Autrey, T.; Shioyama, H.; Xu, Q. Immobilizing Highly Catalytically Active Pt Nanoparticles inside the Pores of Metal–Organic Framework: A Double Solvents Approach *J. Am. Chem. Soc.* **2012**, *134*, 13926-13929.

(27)Kuo, C.-H.; Tang, Y.; Chou, L.-Y.; Sneed, B. T.; Brodsky, C. N.; Zhao, Z.; Tsung, C.-K. Yolk–Shell Nanocrystal@ZIF-8 Nanostructures for Gas-Phase Heterogeneous Catalysis with Selectivity Control *J. Am. Chem. Soc.* **2012**, *134*, 14345-14348.

(28)Ke, F.; Zhu, J.; Qiu, L.-G.; Jiang, X. Controlled Synthesis of Novel Au@MIL-100(Fe) Core-Shell Nanoparticles with Enhanced Catalytic Performance *Chem. Commun.* **2013**, *49*, 1267-1269.

(29)Wang, P.; Zhao, J.; Li, X.; Yang, Y.; Yang, Q.; Li, C. Assembly of ZIF Nanostructures around Free Pt Nanoparticles: Efficient Size-Selective Catalysts for Hydrogenation of Alkenes under Mild Conditions *Chem. Commun.* **2013**, *49*, 3330-3332.

(30)Chen, L.; Chen, H.; Luque, R.; Li, Y. Metal-Organic Framework Encapsulated Pd Nanoparticles: Towards Advanced Heterogeneous Catalysts *Chem. Sci.* **2014**, *5*, 3708-3714.

(31)Chen, L.; Chen, H.; Li, Y. One-Pot Synthesis of Pd@MOF Composites without the Addition of Stabilizing Agents *Chem. Commun.* **2014**, *50*, 14752-14755.

(32)Na, K.; Choi, K. M.; Yaghi, O. M.; Somorjai, G. A. Metal Nanocrystals Embedded in Single Nanocrystals of MOFs Give Unusual Selectivity as Heterogeneous Catalysts *Nano Lett.* **2014**, *14*, 5979-5983.

(33)Zhao, M.; Deng, K.; He, L.; Liu, Y.; Li, G.; Zhao, H.; Tang, Z. Core–Shell Palladium Nanoparticle@Metal–Organic Frameworks as Multifunctional Catalysts for Cascade Reactions *J. Am. Chem. Soc.* **2014**, *136*, 1738-1741.

(34)Liu, H.; Chang, L.; Chen, L.; Li, Y. In Situ One-Step Synthesis of Metal-Organic Framework Encapsulated Naked Pt Nanoparticles without Additional Reductants *J. Mat. Chem. A* **2015**, *3*, 8028-8033.

(35)Chen, L.; Chen, X.; Liu, H.; Li, Y. Encapsulation of Mono-or Bimetal Nanoparticles inside Metal–Organic Frameworks Via in Situ Incorporation of Metal Precursors *Small* **2015**.

(36)Weissermel, K.; Arpe, H.-J. In *Industrial Organic Chemistry*; Wiley-VCH Verlag GmbH: 2008, p 193-215.

(37)Labinger, J. A.; Bercaw, J. E. Understanding and Exploiting C-H Bond Activation *Nature* **2002**, *417*, 507-514.

(38)*This result was obtained from preliminary DFT calculations of isolated C_4 species using the settings specified in computational details.*

(39)Schlögl, R. In *Modern Heterogeneous Oxidation Catalysis*; Wiley-VCH Verlag GmbH & Co. KGaA: 2009, p 1-42.

(40)Chung, Y. G.; Camp, J.; Haranczyk, M.; Sikora, B. J.; Bury, W.; Krungleviciute, V.; Yildirim, T.; Farha, O. K.; Sholl, D. S.; Snurr, R. Q. Computation-Ready, Experimental Metal–Organic Frameworks: A Tool to Enable High-Throughput Screening of Nanoporous Crystals *Chem. Mat.* **2014**, *26*, 6185-6192.

(41)Senkan, S. M. High-Throughput Screening of Solid-State Catalyst Libraries *Nature* **1998**, *394*, 350-353.

(42)Dapprich, S.; Komáromi, I.; Byun, K. S.; Morokuma, K.; Frisch, M. J. A New ONIOM Implementation in Gaussian98. Part I. The Calculation of Energies, Gradients, Vibrational Frequencies and Electric Field Derivatives1 *J. Mol. Struct. Theochem* **1999**, *461–462*, 1-21.

(43)Oxford, G. A. E.; Snurr, R. Q.; Broadbelt, L. J. Hybrid Quantum Mechanics/Molecular Mechanics Investigation of (Salen)Mn for Use in Metal–Organic Frameworks *Ind. Eng. Chem. Res.* **2010**, *49*, 10965-10973.

(44)Hirao, H.; Ng, W. K. H.; Moeljadi, A. M. P.; Bureekaew, S. Multiscale Model for a Metal–Organic Framework: High-Spin Rebound Mechanism in the Reaction of the Oxoiron(IV) Species of Fe-MOF-74 *ACS Catal.* **2015**, 3287-3291.

(45)Chung, L. W.; Sameera, W. M. C.; Ramozzi, R.; Page, A. J.; Hatanaka, M.; Petrova, G. P.; Harris, T. V.; Li, X.; Ke, Z.; Liu, F.; Li, H.-B.; Ding, L.; Morokuma, K. The ONIOM Method and Its Applications *Chem. Rev.* **2015**.

(46)Zhang, C. J.; Hu, P. Methane Transformation to Carbon and Hydrogen on Pd(100): Pathways and Energetics from Density Functional Theory Calculations *J. Chem. Phys.* **2002**, *116*, 322-327.

(47)Weaver, J. F.; Hinojosa Jr, J. A.; Hakanoglu, C.; Antony, A.; Hawkins, J. M.; Asthagiri, A. Precursor-Mediated Dissociation of n-butane on a PdO(101) Thin Film *Catal. Today* **2011**, *160*, 213-227.

(48)Trinchero, A.; Hellman, A.; Grönbeck, H. Methane Oxidation over Pd and Pt Studied by DFT and Kinetic Modeling *Surf. Sci.* **2013**, *616*, 206-213.

(49)Chin, Y.-H.; Buda, C.; Neurock, M.; Iglesia, E. Consequences of Metal–Oxide Interconversion for C–H Bond Activation During CH_4 Reactions on Pd Catalysts *J. Am. Chem. Soc.* **2013**, *135*, 15425-15442.

(50)Weaver, J. F.; Hakanoglu, C.; Antony, A.; Asthagiri, A. High Selectivity for Primary C–H Bond Cleavage of Propane σ-Complexes on the PdO(101) Surface *J. Am. Chem. Soc.* **2011**, *133*, 16196-16200.

(51)Hakanoglu, C.; Zhang, F.; Antony, A.; Asthagiri, A.; Weaver, J. F. Selectivity in the Initial C-H Bond Cleavage of n-butane on PdO(101) *Phys. Chem. Chem. Phys.* **2013**, *15*, 12075-12087.

(52)Kresse, G.; Hafner, J. Ab Initio Molecular Dynamics for Liquid Metals *Phys. Rev. B* **1993**, *47*, 558-561.

(53)Kresse, G.; Hafner, J. Ab Initio Molecular-Dynamics Simulation of the Liquid-Metal/Amorphous-Semiconductor Transition in Germanium *Phys. Rev. B* **1994**, *49*, 14251-14269.

(54)Kresse, G.; Furthmüller, J. Efficiency of Ab-Initio Total Energy Calculations for Metals and Semiconductors Using a Plane-Wave Basis Set *Comput. Mat. Sci.* **1996**, *6*, 15-50.

(55)Kresse, G.; Furthmüller, J. Efficient Iterative Schemes for Ab Initio Total-Energy Calculations Using a Plane-Wave Basis Set *Phys. Rev. B* **1996**, *54*, 11169-11186.

(56)Perdew, J. P.; Burke, K.; Ernzerhof, M. Generalized Gradient Approximation Made Simple *Phys. Rev. Lett.* **1996**, *77*, 3865-3868.

(57)Blöchl, P. E. Projector Augmented-Wave Method *Phys. Rev. B* **1994**, *50*, 17953-17979.

(58)Kresse, G.; Joubert, D. From Ultrasoft Pseudopotentials to the Projector Augmented-Wave Method *Phys. Rev. B* **1999**, *59*, 1758-1775.

(59)Grimme, S. Semiempirical GGA-Type Density Functional Constructed with a Long-Range Dispersion Correction *J. Comput. Chem.* **2006**, *27*, 1787-1799.

(60)Ho, K. M.; Fu, C. L.; Harmon, B. N.; Weber, W.; Hamann, D. R. Vibrational Frequencies and Structural Properties of Transition Metals Via Total-Energy Calculations *Phys. Rev. Lett.* **1982**, *49*, 673-676.

(61)Dutta, B. N.; Dayal, B. Lattice Constants and Thermal Expansion of Palladium and Tungsten up to 878 °C by X-Ray Method *phys. stat. sol. (b)* **1963**, *3*, 2253-2259.

(62)"Material Studio"; Accelrys Software Inc.: San Diego, CA 92121, USA, 2001-2011.

(63)Blöchl, P. E.; Jepsen, O.; Andersen, O. K. Improved Tetrahedron Method for Brillouin-Zone Integrations *Phys. Rev. B* **1994**, *49*, 16223-16233.

(64)Henkelman, G.; Arnaldsson, A.; Jónsson, H. A Fast and Robust Algorithm for Bader Decomposition of Charge Density *Comput. Mat. Sci.* **2006**, *36*, 354-360.

(65)Tang, W.; Sanville, E.; Henkelman, G. A Grid-Based Bader Analysis Algorithm without Lattice Bias *J. Phys. Cond. Matter* **2009**, *21*, 084204.

(66)Park, K. S.; Ni, Z.; Côté, A. P.; Choi, J. Y.; Huang, R.; Uribe-Romo, F. J.; Chae, H. K.; O'Keeffe, M.; Yaghi, O. M. Exceptional Chemical and Thermal Stability of Zeolitic Imidazolate Frameworks *Proc. Natl Acad. Sci.* **2006**, *103*, 10186-10191.

(67)Zhang, C.; Lively, R. P.; Zhang, K.; Johnson, J. R.; Karvan, O.; Koros, W. J. Unexpected Molecular Sieving Properties of Zeolitic Imidazolate Framework-8 *J. Phys. Chem. Lett.* **2012**, *3*, 2130-2134.

(68)Gee, J. A.; Chung, J.; Nair, S.; Sholl, D. S. Adsorption and Diffusion of Small Alcohols in Zeolitic Imidazolate Frameworks ZIF-8 and ZIF-90 *J. Phys. Chem. C* **2013**, *117*, 3169-3176.

(69)Zhang, K.; Zhang, L.; Jiang, J. Adsorption of C_1–C_4 Alcohols in Zeolitic Imidazolate Framework-8: Effects of Force Fields, Atomic Charges, and Framework Flexibility *J. Phys. Chem. C* **2013**, *117*, 25628-25635.

(70)Hirschfelder, J. O.; Curtiss, C. F.; Bird, R. B. *Molecular Theory of Gases and Liquids*; Wiley: New York, 1954.

(71)Eichler, A.; Mittendorfer, F.; Hafner, J. Precursor-Mediated Adsorption of Oxygen on the (111) Surfaces of Platinum-Group Metals *Phys. Rev. B* **2000**, *62*, 4744-4755.

(72)Todorova, M.; Reuter, K.; Scheffler, M. Oxygen Overlayers on Pd(111) Studied by Density Functional Theory† *J. Phys. Chem. B* **2004**, *108*, 14477-14483.

(73)Pallassana, V.; Neurock, M.; Hansen, L. B.; Hammer, B.; Nørskov, J. K. Theoretical Analysis of Hydrogen Chemisorption

on Pd(111), Re(0001) and PdML/Re(0001), ReML/Pd(111) Pseudomorphic Overlayers *Phys. Rev. B* **1999**, *60*, 6146-6154.

(74)Watson, G. W.; Wells, R. P. K.; Willock, D. J.; Hutchings, G. J. A Comparison of the Adsorption and Diffusion of Hydrogen on the {111} Surfaces of Ni, Pd, and Pt from Density Functional Theory Calculations *J. Phys. Chem. B* **2001**, *105*, 4889-4894.

(75)Herron, J. A.; Tonelli, S.; Mavrikakis, M. Atomic and Molecular Adsorption on Pd(111) *Surf. Sci.* **2012**, *606*, 1670-1679.

(76)Mitsui, T.; Rose, M. K.; Fomin, E.; Ogletree, D. F.; Salmeron, M. Hydrogen Adsorption and Diffusion on Pd(111) *Surf. Sci.* **2003**, *540*, 5-11.

(77)Rose, M. K.; Borg, A.; Dunphy, J. C.; Mitsui, T.; Ogletree, D. F.; Salmeron, M. Chemisorption of Atomic Oxygen on Pd(111) Studied by Stm *Surf. Sci.* **2004**, *561*, 69-78.

(78)Getman, R. B.; Xu, Y.; Schneider, W. F. Thermodynamics of Environment-Dependent Oxygen Chemisorption on Pt(111) *J. Phys. Chem. C* **2008**, *112*, 9559-9572.

(79)Getman, R. B.; Schneider, W. F. Dft-Based Coverage-Dependent Model of Pt-Catalyzed No Oxidation *ChemCatChem* **2010**, *2*, 1450-1460.

(80)Simmons, G. W.; Wang, Y. N.; Marcos, J.; Klier, K. Oxygen Adsorption on Palladium(100) Surface: Phase Transformations and Surface Reconstruction *J. Phys. Chem.* **1991**, *95*, 4522-4528.

(81)Saidy, M.; Warren, O. L.; Thiel, P. A.; Mitchell, K. A. R. A Structural Refinement with Leed for the Pd(100)–(√5×√5)R27°-O Surface *Surf. Sci.* **2001**, *494*, L799-L804.

(82)Zheng, G.; Altman, E. I. The Oxidation Mechanism of Pd(100) *Surf. Sci.* **2002**, *504*, 253-270.

(83)Senftle, T. P.; Meyer, R. J.; Janik, M. J.; van Duin, A. C. T. Development of a ReaxFF Potential for Pd/O and Application to Palladium Oxide Formation *J. Chem. Phys.* **2013**, *139*, 044109.

(84) *No calculations were done for "2-" C_4 species with the pore, because steric constraints do not allow the activation of the secondary carbon of n-butane.*

(85)Morikawa, Y.; Ishii, H.; Seki, K. Theoretical Study of N-Alkane Adsorption on Metal Surfaces *Phys. Rev. B* **2004**, *69*, 041403.

(86)Lee, K.; Morikawa, Y.; Langreth, D. C. Adsorption of N-Butane on Cu(100), Cu(111), Au(111), and Pt(111): Van Der Waals Density-Functional Study *Phys. Rev. B* **2010**, *82*, 155461.

(87) *The only exception was for the '‡' case in Table 7, where one of the pre-adsorbed oxygens moved from its original positions due to 1-butenyl adsorption.*

TOC Figure
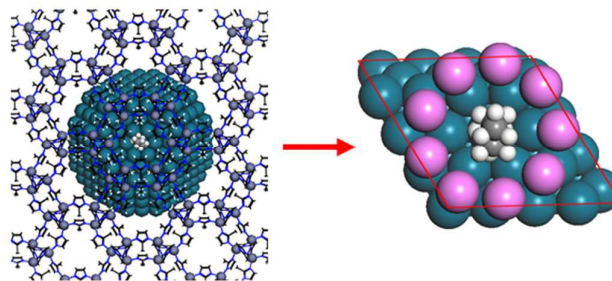
A surrogate pore mimics the steric constraints provided by a MOF on n-butane in a MOF-encapsulated metal catalyst